


Differences in vegetation index values using measurements from two azimuth and multiple zenith viewing angles**

Hyun-Dong Moon^{1,2}, Hyunki Kim^{1,3}, Yuna Cho^{1,2}, Euni Jo^{1,2}, Jae-Hyun Ryu⁴, Hoyong Ahn⁴, Sang-Il Na⁴,
Kyung-Do Lee⁴, Yangwon Lee⁵, and Jaeil Cho^{1,2} 

¹Department of Applied Plant Science, Chonnam National University, Gwangju 61186, Republic of Korea

²BK21 FOUR Center for IT-Bio Convergence System Agriculture, Chonnam National University, Gwangju 61186, Republic of Korea

³National Institute of Crop Sciences, Rural Development Administration, Wanju 55365, Republic of Korea

⁴National Institute of Agricultural Sciences, Rural Development Administration, Wanju 55365, Republic of Korea

⁵Department of Spatial Information Engineering, Pukyong National University, Busan 48513, Republic of Korea

Received August 14, 2023; accepted December 27, 2023

Abstract. Vegetation indices based on selected wavelength reflectance measurements are used to represent crop growth and physiological conditions. However, it has been determined that the anisotropic properties of the crop canopy surface can govern both the spectral reflectance and vegetation indices. In this study, in order to investigate how crop surface reflectance and vegetation indices varied according to the direction of the light source and sensor viewing, a hyper-spectrometer of visible to near-infrared wavelengths mounted on a field goniometer was used at vegetative and reproductive growth stages in rice paddy. It was found that most of the wavelength reflectance measurements produced by the sparse vegetation cover fraction were not sensitive to solar-illumination and sensor-viewing angles. In addition, the reflectance of visible wavelengths was found to be less sensitive to the solar and sensor angles than the red-edge and near-infrared wavelengths. The lowest normalized difference vegetation index value in a day occurred at the nadir sensor-viewing angle before rice heading, but after heading, when ripened grains began to bow, the lowest value was recorded at the sensor zenith angle of 25°. Enhanced vegetation index measurements were found to be more sensitive to the direction of sensor viewing and less affected by sun glint than normalized difference vegetation index measurements. Additional field observation measurements should increase our level of understanding of how vegetation indices change on anisotropic crop surfaces.

Keywords: field goniometer, spectral reflectance, vegetation index, sensor-viewing angle, solar-illumination angle

1. INTRODUCTION

As agriculture has advanced, cultivation and breeding technologies have been developed to increase crop productivity. In recent times, with the development of digital agricultural technology, crop growth can now be detected and analysed rapidly and continuously, in particular by using remote sensing techniques (Lee *et al.*, 2017). Vegetation indices derived from the selective wavelength reflectance of crop canopy surfaces are widely used to assess crop growth and monitor the occurrence and extent of stress on agricultural land (Kamble *et al.*, 2013; Na *et al.*, 2016). Thus, a better understanding of vegetation indices is necessary in order to accurately measure canopy reflectance with the solar incident irradiance on open field crops as well as the radiation reflected from the canopy surfaces.

However, since the spectral reflectance of crop canopy surfaces has anisotropic properties that depend on the direction of the light source and the relative sensor position, vegetation indices may differ without any change in crop condition (Ma *et al.*, 2021). Consequently, even if soil and vegetation surface properties remain constant, the vegetation indices may be determined by both the solar zenith and

*Corresponding author e-mail: chojaeil@gmail.com

**This work was carried out with the support of "Cooperative Research Program for Agriculture Science and Technology Development (Project No. RS-2021-RD009991)" by the Rural Development Administration.

azimuth angles and sensor observation angle. This problem is extensive enough to confound the accurate analyses of crop growth and physiological conditions.

Therefore, in order to obtain accurate estimates of crop growth or stress from the observed vegetation index in open field conditions, the anisotropic properties of reflectance according to the sensor-viewing direction and solar movement during the day should be considered (Queally *et al.*, 2022). A numerical simulation of the bidirectional reflectance distribution function (BRDF) model is often used to correct land surface reflectance anisotropy through the physical relationship between the light source direction, the observed sensor angle, and the scattering of surface reflectance (Gao *et al.*, 2003; Li *et al.*, 2021; Zhang *et al.*, 2014a). However, because such simulations are determined on the basis of simple crown shapes (*e.g.*, cone, cylinder, ellipsoid, and cylinder) for estimating the relevant isometric, geometric, and volumetric parameters (Zhang *et al.*, 2014a), the model should be validated in order to complement the performance of reflectance correction by using reflectance values measured under the most diverse incident light and sensor-viewing directions (Li *et al.*, 2010). Furthermore, considering that the vegetation indices derived from most satellite reflectance measurements are often used without BRDF correction (Yan *et al.*, 2022), it will be necessary to evaluate the extent of the anisotropic effects in specific crops and those occurring during particular growing seasons to enhance understanding of vegetation indices.

The goniometer is an instrument that either measures an angle or allows an object to be rotated to a precise angular position, to obtain the observed reflectance according to various light and sensor angle positions in open fields of vegetation (Sandmeier and Itten, 1999). A number of previous studies have utilized goniometers outdoors. However, despite rice being a crucial food crop in Asia, there are currently very few studies that have been used to evaluate the anisotropic reflectance in rice fields by using a goniometer to measure it.

Sun *et al.* (2017) constructed a vertical axis rotating goniometer by modifying a large camera tripod. The reflectance of soil and rice was observed from nine angles at a height of 2 m. Additionally, the reflectance measurements at four wavelengths were compared with the leaf area index (LAI). However, maintaining the stability of the goniometer body is challenging in an outdoor environment where observation angles frequently change, as the goniometer is supported by a camera tripod.

Suomalainen *et al.* (2009) compared reflectance measurements at different sensor-viewing angles for an outdoor, snowy surface using a vertical axis rotating goniometer with an adjustable height of between 155 and 265 cm. This system is unique in that the centre of gravity is placed as close to the ground as possible so that the goniometer can reliably maintain the selected angle and level, even out-

doors. However, as was true of the general vertical axis rotation system, the goniometer must be moved to change the sensor azimuth angle.

Sandmeier and Itten (1999) and Schill *et al.* (2004) installed a hyper-spectrometer on a hemispherical goniometer with a diameter of about 2 m and found that it was possible to observe the surface reflectance for each wavelength band at all sensor azimuth and zenith angles according to changes in the solar azimuth and zenith angle. Even though the advantage of being able to assess the distribution of all of the scattering reflectance values without any sensor-viewing restrictions is especially significant, this system is very expensive and difficult to install, and it must again be emphasized that there is some concern about damaging vegetation.

The studies examining the anisotropic properties of ground vegetation reflectance are not yet adequate. In addition, field goniometer experiments that involve continuously observing canopy reflectance across different plant growth stages are very rare. In this study, a hyper-spectrometer installed on a field goniometer was used to measure the surface reflectance of visible and near infrared (NIR) wavelengths at different solar and sensor angles across two crop growth stages in rice paddies.

2. MATERIALS AND METHODS

In this study, the goniometer design of Suomalainen *et al.* (2009) was modified for use in rice paddy conditions for the purposes of the experiment. The boom extending upward from the centre of the goniometer was connected to an angle-adjusting bracket that rotated 180° left or right. Thus, the rotating boom could be fixed at any angle of the bracket, this was made from stainless-steel plates with a 2 mm thickness. The length of the upward boom was set at 188 cm to accommodate the height of the rice plant (Fig. 1a). Another boom originating from the end of the upward boom extended 122 cm horizontally, and a downward facing fibre of a hyper-spectrometer was installed at the end of this horizontal boom to observe the rice paddy.

The goniometer, which was made from lightweight black aluminium frames, was easy to move and minimized the effect of diffuse reflectance from the structure. A stainless-steel plate positioned at the bottom of the goniometer prevented the bending of the bottom of the structure and allowed for easy levelling in the field. During observations, a heavy object (*e.g.*, a sandbag) was placed on the bottom plate for stability.

The hyper-spectrometer (RoX, JB Hyperspectral Devices, Düsseldorf, Germany) installed on the goniometer was used to measure both the incident and reflected radiant energy at wavelengths between 400 and 950 nm. The hyper-spectrometer was calibrated with a white hemispherical reflectance with > 98% reflectivity. The fields of view of the upward- and downward-facing fibres incident and

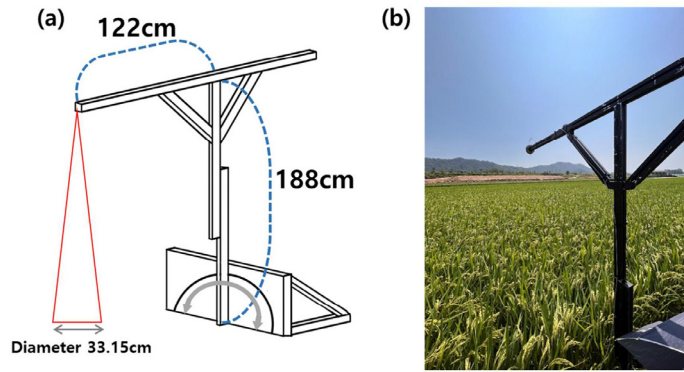


Fig. 1. Design of the field mobile goniometer used in this study (a), observation of the rice paddy conducted on September 7, 2022 (b).

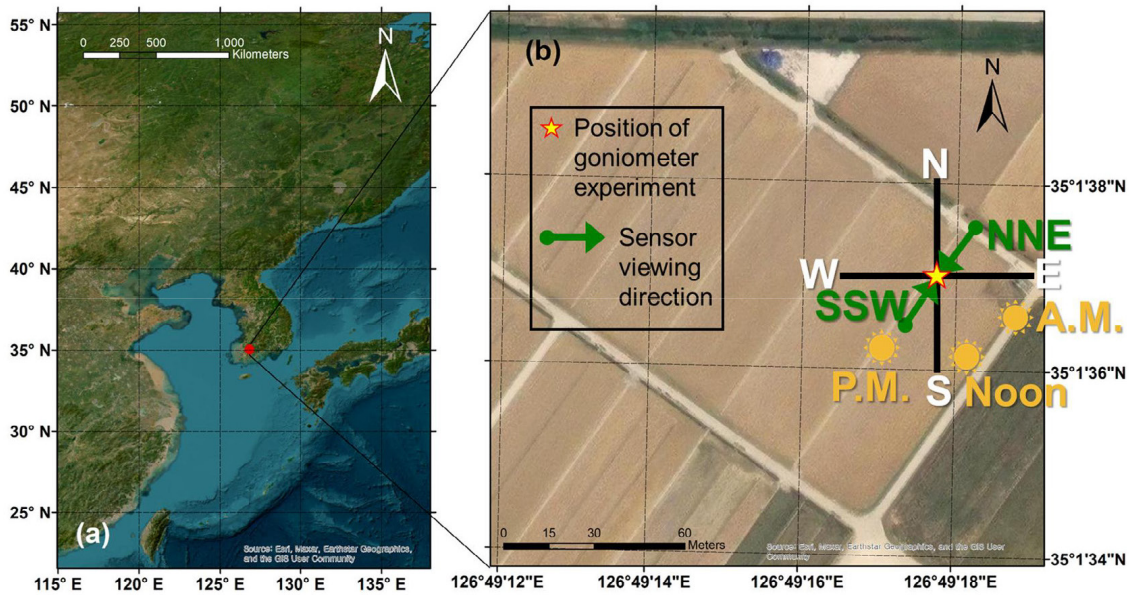


Fig. 2. Location of the field goniometer observation station in Naju City (a) and azimuth angles of sensor viewing and solar illumination used for observing by the field goniometer (b).

reflection probes were 20 and 180°. While the downward-facing fibre was installed on the boom of the goniometer, another optical fibre which was upward-facing stood apart from the goniometer. Assuming that there were no rice plants, the observation footprint area at the nadir-viewing angle of the downward-facing fibre was 33.15 cm in radius at its maximum height. The size of the footprint area varied with the rotation of the central boom of the goniometer. For example, at a viewing angle of 50°, the footprint was an ellipse of 33.14 cm in the minor axis and 65.29 cm in the major axis.

The study area (35°01'36.94"N, 126°49'18.01"E) was a rice paddy field managed by the Jeollanamdo Agricultural Research and Extension Services (JARES) in Naju City, Republic of Korea (Fig. 2a). The rice variety used was Gangdaechan of *Oryza sativa* L. *japonica*, which was developed by the JARES. The mid-late maturing Gangdaechan cultivar typically has vertical leaves and its

maximum height is approximately 1 m. The rice planting density was 15 × 30 cm. Planting was performed on June 7, 2022, with the rice heading stage beginning on August 20 and harvesting taking place on October 20.

A single observation took place over the course of a single day, in all 6 days of observations occurred. Three of these days occurred during the vegetative growth stage, and the other 3 days occurred after the heading stage. Although the soil in the rice paddy studied is clay, the first, second, and sixth observations took place under drained conditions. The third, fourth, and fifth were carried out under flooded conditions. The weather during all observations was sunny.

The goniometer was positioned on the footpath between the rice paddies running from north-northeast (NNE) to south-southwest (SSW) (Fig. 1b). Thus, the boom was also rotated from the NNE and SSW directions (Fig. 2b). One-time observations were conducted sequentially at five sensor zenith angles of -50 and -25° in the NNE direction,

Table 1. Equations and properties of vegetation indices used in this study

Vegetation index	Equation	Property
Normalized difference vegetation	$NDVI = (R_{800} - R_{668}) / (R_{800} + R_{668})$	Structural
Enhanced vegetation	$EVI = 2.5 (R_{800} - R_{668}) / (R_{800} + 6 R_{668} - 7.5 R_{475} + 1)$	
MERIS terrestrial chlorophyll	$MTCI = (R_{740} - R_{717}) / (R_{717} - R_{668})$	Biochemical
Normalized difference red edge	$NDRE = (R_{800} - R_{717}) / (R_{800} + R_{717})$	
Photochemical reflectance	$PRI = (R_{531} - R_{570}) / (R_{531} + R_{570})$	Physiological
Chlorophyll carotenoid	$CCI = (R_{531} - R_{668}) / (R_{531} + R_{668})$	

0° in the nadir direction, and 25 and 50° in the SSW direction. The value at each sensor zenith angle was obtained using the average of measurements repeated three-times within a time scale of about one minute. The one-day observations took place over three-time intervals: 10:00-11:00, 12:00-13:00, and 14:00-15:00.

In this goniometer experiment, the vegetation indices used were the normalized difference vegetation index (NDVI), enhanced vegetation index (EVI), MERIS terrestrial chlorophyll index (MTCI), normalized difference red edge (NDRE), photochemical reflectance index (PRI), and the chlorophyll carotenoid index (CCI). NDVI and EVI are related to the structure and biomass of vegetation, while MTCI and NDRE are sensitive to the chlorophyll content. PRI and CCI are suited to providing a representation of physiological states, particularly those related to photosynthetic efficiency. Table 1 shows the equation used to calculate each vegetation index, and R represents the reflectance wavelength. In addition, the error rate occurring due to sun glint was also investigated. When the solar-illumination and sensor-viewing positions were at their most similar, and if the reflectance value appeared to be distinct from the reflectance at a different angle, this was considered to be the result of sun glint.

$$ER = \frac{v_{measured} - v_{true}}{v_{true}} 100,$$

where: ER is the error rate (%), $v_{measured}$ is the value measured by the hyper-spectrometer of the goniometer, and v_{true} is the true value used to evaluate the measured value. In the case of sun glint error analysis, the true value was considered to be the value estimated using linear correlation analysis with the reflectance of the two angles being 25° greater and less than the angle which occurred due to sun glint. For a comparison of NDVI and EVI, the value measured for the nadir sensor position at noon was set as the true.

3. RESULTS AND DISCUSSION

Figure 3 shows the seven reflectance values of the wavelengths used (*i.e.*, 475, 531, 570, 668, 717, 740, and 800 nm) in calculating the NDVI, EVI, MTCI, NDRE, PRI, and CCI according to five sensor zenith angles and three solar zenith angles at five rice growth stages. The reflectance

results from the goniometer experiment are determined by differences in: 1) the absorption of radiation wavelengths according to the physiological condition and structural state of the leaves (Ryu *et al.*, 2020); 2) the canopy structure and the direction in which the sensor was facing and also the degree of solar illumination (Ma *et al.*, 2021; Towers and Poblete-Echeverría, 2021); and 3) light penetration into and escape from the canopy (Qiu *et al.*, 2016).

In general terms, the lowest reflectance value measured in a day occurred at the time of nadir sensor-viewing angle. This is consistent with the result produced by a rice canopy, as determined by Sun *et al.* (2017). However, before rice heading, as compared to both red-edge and NIR wavelengths, the reflectance of the visible wavelengths (475, 531, 570, and 668 nm) was lower and less sensitive to the sensor-viewing and solar-illumination directions.

As the wavelength increased, the variations in reflectance became relatively larger according to the sensor zenith angle. In addition, the reflectance values increased after rice heading (September 7, 20, and 29), being notably smaller in the blue (475 nm) and red (668 nm) bands and larger in the red-edge (717 and 740 nm) and NIR (800 nm) regions. At a larger sensor zenith angle, the pathway of light penetrating into the crop canopy will be longer than it is for the smaller sensor zenith angle. Thus, the red-edge and NIR regions, which produced high reflectance values on canopies, might be more sensitive to viewing angles than the visible wavelengths.

Among all of the wavelengths used and the directions of solar illumination, the reflectance values that were determined using the five sensor zenith angles were higher and more varied in the afternoon (red line in Fig. 3) of September 29, during the ripening stage. This pattern may be caused by the scatter created by the bowing of the ripening grains at a particular backward-nadir-forward sensor-viewing position in the afternoon (Fig. 2).

Again, on September 29, the blue (475 nm) and red (668 nm) wavelengths used in the morning and noon measurements (blue and green lines in Fig. 3) showed that the backward-scattered reflectance detected at sensor zenith angles of 25 and 50° was higher than the forward-scattered reflectance at -50 and -25°. Because of the gap in the canopy surface filled by bowing grains, less solar irradiation can

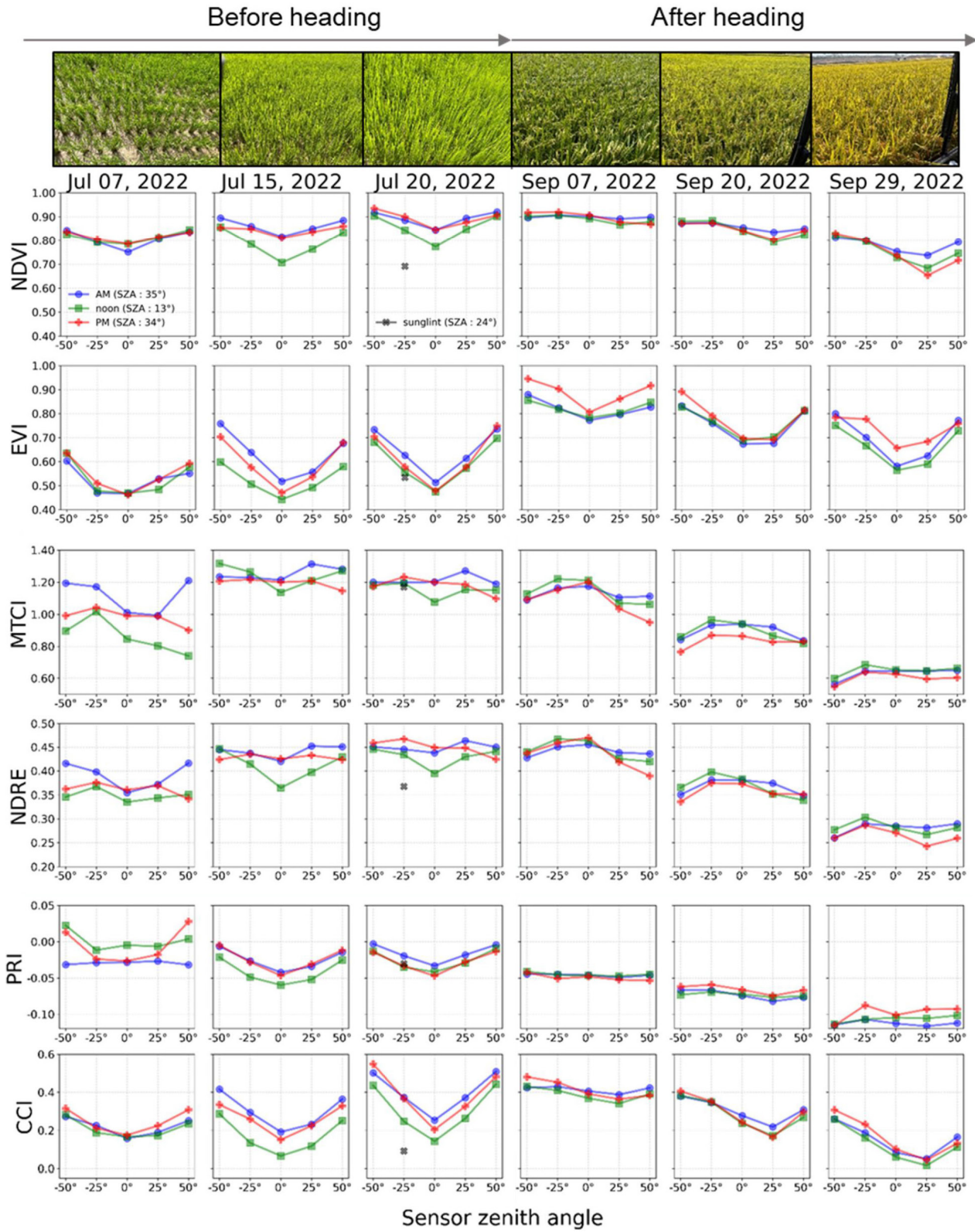


Fig. 3. Reflectance observed in rice paddies across growth periods before and after heading. The red, green, and blue lines show the measurements in the morning sensor zenith angle (SZA: 35°), noon (SZA: 13°), and afternoon (SZA: 34°), respectively.

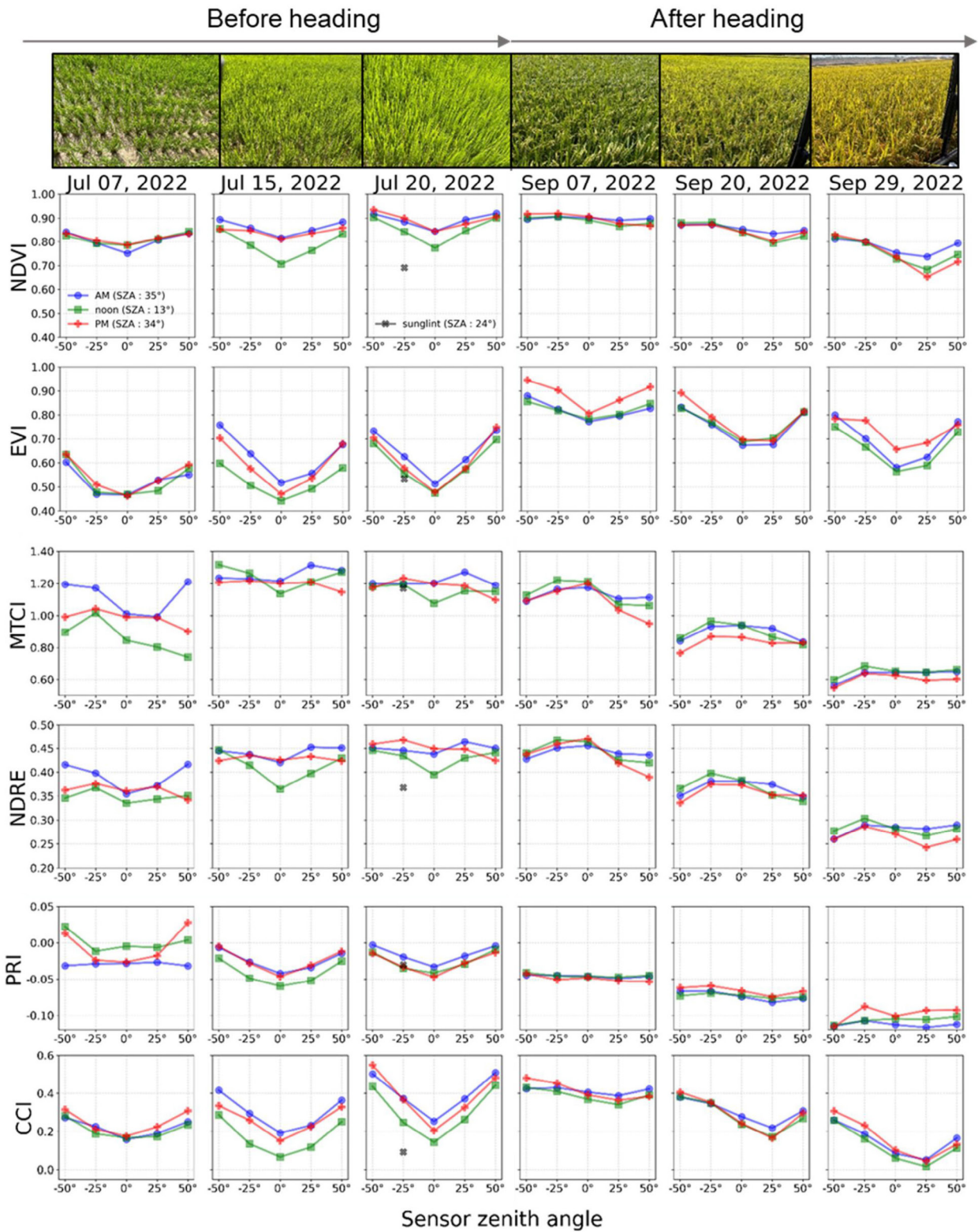


Fig. 4. Vegetation indices observed in rice paddies across growth periods before and after heading (also see Fig. 3).

penetrate the canopy, and it is instead reflected backward at the canopy surface. In addition, the penetrated radiation might not escape from inside the canopy.

Figure 4 shows the values of NDVI, EVI, MTCI, NDRE, PRI, and CCI according to five sensor zenith angles and three solar zenith angles at five rice growth stages. The values of NDVI increased with rice growth but decreased after rice heading which complied with previous studies concerning time series crop monitoring (e.g., Ryu *et al.*, 2020). The lowest NDVI value for one observation day occurred at the time of the nadir sensor-viewing angle. The NDVI values determined in the morning, noon, and afternoon were different, but they were found to be similar for each measurement day. This is consistent with the results of Ma *et al.* (2021) despite the experiment being conducted in a maize field. However, on July 15 and 20, the NDVI values at noon (green line in Fig. 4) were smaller than those in the morning and afternoon, but their variations were larger according to the sensor zenith angles.

The lower sensitivity of NDVI to sensor-viewing and solar-illumination angles on July 7 than on July 15 and 20 may have been caused by the low surface cover fraction of rice plants, which is particularly facilitated by the vertical canopy shape of the rice plant (Sinclair and Sheehy, 1999). However, although the plants had grown more (July 15 and 20), the NDVI value at noon, during which there was a small solar zenith angle, could be as low as that which occurred at the nadir sensor-viewing angle on July 7. On September 7 the NDVI was determined by the top-most surface of the canopy because it was dense and uniform. Thus, the measurements taken on this day may have been insensitive to changes occurring in sensor-viewing angle and solar illumination. On the other hand, when the roughness of the canopy surface increased as the rice began to bow downward (September 20 and 29) (Zhang *et al.*, 2014b), the variation in the NDVI could have been influenced by variations in sensor-viewing angle despite the dense canopy, which conforms to the strong relationship found between NDVI and the vegetation cover fraction in

previous studies (e.g., Campos *et al.*, 2014; Shafian *et al.*, 2018). At this ripening stage, the lowest NDVI occurred at the sensor zenith angle of 25° among all of the goniometer setting angles applied.

The patterns of the EVI were similar to those of the NDVI, but the EVI was found to be more sensitive to the direction of sensor viewing. Although the EVI uses blue wavelengths to lessen the effect of soil contamination as compared to the NDVI (Liu and Huete, 1995), the components in the rice canopies which affect such wavelengths may have mathematically offset the pattern of red wavelengths in the EVI equation because both blue and red belong to the wavelength regions related to photosynthesis. As a consequence, NIR features could be primarily represented in the EVI.

Figure 5 shows the error rate according to the directions of sensor viewing and solar illumination, the comparison between NDVI and EVI is particularly noteworthy. Although the errors were different for each rice growth period, the EVI was found to have a higher error than the NDVI. This was similar to the results achieved by Matsushita *et al.* (2007) which indicated that the EVI is more sensitive to topographic conditions than the NDVI. Indeed, the path length of the light which penetrated into the canopy will be affected by variations in sensor-viewing angle and solar illumination through sensor operation, latitude, time/season, and topography. This difference in light path length may affect the EVI more than the NDVI because the EVI was developed to improve sensitivity to biomass by removing the soil background signal.

Even though there is no common wavelength used to determine MTCI and NDRE, which were developed to estimate plant chlorophyll content (Dash and Curran, 2007; Sharifi, 2020), these two vegetation indices demonstrated similar patterns with regard to sensor-viewing and solar-illumination directions. Both indices exhibited relatively large differences according to the solar time, particularly in July, when the canopy was relatively open.

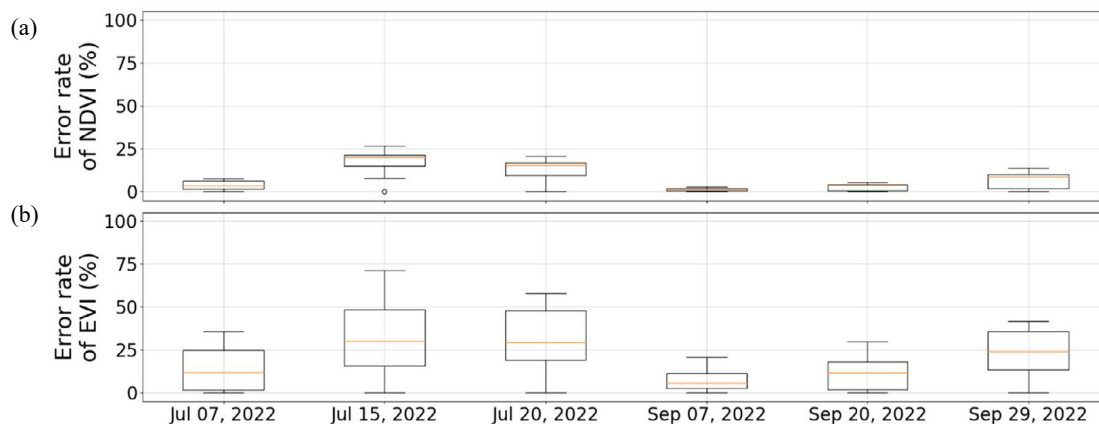


Fig. 5. Error rate (%) according to the directions of sensor viewing and solar illumination for (a) NDVI and (b) EVI (also see Fig. 4).

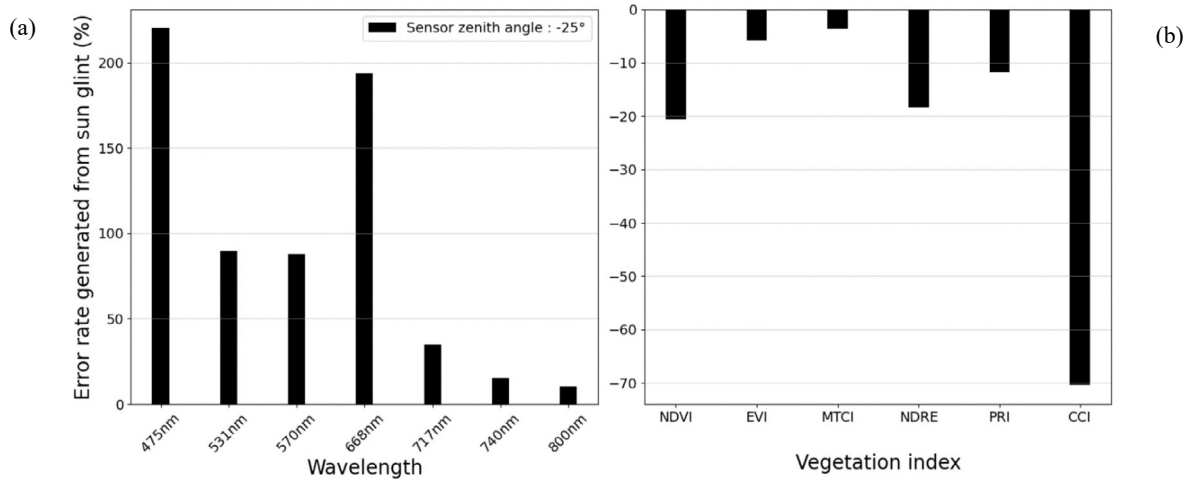


Fig. 6. Outcome of dividing the sun-glint value by the estimated true value of the (a) band reflectance and (b) vegetation indices in the goniometer experiment.

Unlike other vegetation indices, the PRI may be sensitive to changes in solar irradiance during the day. Solar radiation stress generally reduces the PRI (Gamon *et al.*, 1992), as it induces physiological stress. Thus, it was predicted that the PRI measured using backward-scattered reflectance at sensor zenith angles of 25 and 50° would be lower than that of the forward-scattered reflectance at -50 and -25°. However, before rice heading, the PRI changes due to sensor-viewing directions were symmetrical for the backward and forward directions. In addition, after rice heading, the PRI values were less sensitive to the direction of sensor viewing and solar illumination. In the case of the CCI, which was determined using 531 nm like the PRI (Gamon *et al.*, 2016), backward- and forward-scattering cases also exhibited a symmetrical pattern in the pre-heading stage; however, after rice heading, the CCI, which, like the NDVI, was determined using NIR, was found to be lower under backward-scattered reflectance than under forward-scattered reflectance conditions, particularly at the sensor zenith angle of 25°.

Sun glint, or the direct sunlight reflection off a water surface toward the optical sensor viewing of the surface, interrupts the observation of vegetation indices in rice fields (Ortega-Terol *et al.*, 2017). The observation at a -25° viewing angle at 14:00 on July 20 showed evidence of sun glint (gray rectangle marker in Figs 3 and 4). Even though sun glint occurred at 14:00, observations before and after 14:00 (*i.e.*, at 12:00 and 15:00) may be assumed to be free of sun glint. Thus, the true value of the 14:00 measurements without sun glint may be regarded as the average of the observed values at 12:00 and 15:00.

Figure 6 shows the intensity of sun glint, it is represented by the ratio of the sun-glint value to the estimated true value using seven reflectance wavelengths and six vegetation indices. The blue and green wavelengths were found to be sensitive to sun glint, while the red-edge and

NIR wavelengths exhibited smaller changes. The lower reflectance values of the water surface in the NIR region as compared to those produced by visible light is consistent with the findings of Jain and Singh (2003). In addition, the EVI and MTCI were less affected by sun glint, but the CCI experienced large changes due to sun glint.

4. CONCLUSIONS

1. The visible, red-edge, and NIR wavelength reflectance and vegetation indices of rice paddies showed different sensitivities to the applied sensor-viewing and solar-illumination angles. However, such features were also altered by changes in the canopy structure and pigments present at different growth stages.

2. Most wavelength reflectance on sparse canopy cover was found to be less sensitive to the applied sensor-viewing and solar-illumination angles. It is most likely that the reason for this is that the light penetrating and reflecting within the canopy is not significantly disturbed by the crops that do not cover the ground.

3. At nadir sensor-viewing and small solar zenith angles, the value of most reflectance measurements was found to be lower. This is consistent with previous research findings that light can penetrate deeper into a rice canopy with vertical canopy structures.

4. Because the roughness of the rice canopy changed due to the ripening of the grains after rice heading, the reflectance was affected by the sensor-viewing and solar-illuminating angles. Specifically, reflectance was found to be higher in the red-edge and NIR wavelengths than in the visible wavelengths.

5. The lowest normalized difference vegetation index value in a day occurred at the nadir sensor-viewing angle before rice heading, but after heading, the lowest value was recorded at the sensor zenith angle of 25° as the ripened grains began to bow. The patterns of the enhanced

vegetation index were similar to those of the normalized difference vegetation index, but the enhanced vegetation index was found to be more sensitive to the direction of sensor viewing.

6. The effect of sun glint on the reflectance of the paddy water surface was more pronounced in the blue and red wavelengths than in the red-edge and NIR wavelengths. The enhanced vegetation index was found to be less sensitive to sun glint than the normalized difference vegetation index.

Conflicts of Interest: The authors declare no conflict of interest.

5. REFERENCES

- Campos I., Neale C.M., López M.L., Balbontín C., and Calera A., 2014. Analyzing the effect of shadow on the relationship between ground cover and vegetation indices by using spectral mixture and radiative transfer models. *J. Appl. Remote Sens.*, 8(1), 83562-83562, <https://doi.org/10.1117/1.JRS.8.083562>
- Dash J., and Curran P.J., 2007. Evaluation of the MERIS terrestrial chlorophyll index (MTCI). *Adv. Space Res.*, 39(1), 100-104, <https://doi.org/10.1016/j.asr.2006.02.034>
- Gamon J.A., Penuelas J., and Field C.B., 1992. A narrow-waveband spectral index that tracks diurnal changes in photosynthetic efficiency. *Remote Sens. Environ.*, 41(1), 35-44, [https://doi.org/10.1016/0034-4257\(92\)90059-S](https://doi.org/10.1016/0034-4257(92)90059-S)
- Gamon J.A., Huemmrich K.F., Wong C.Y., Ensminger I., Garrity S., Hollinger D.Y., Noormets A., and Peñuelas J., 2016. A remotely sensed pigment index reveals photosynthetic phenology in evergreen conifers. *Proc. Natl. Acad. Sci.*, 113(46), 13087-13092, <https://doi.org/10.1073/pnas.1606162113>
- Gao F., Schaaf C.B., Strahler A.H., Jin Y., and Li X., 2003. Detecting vegetation structure using a kernel-based BRDF model. *Remote Sens. Environ.*, 86(2): 198-205, [https://doi.org/10.1016/S0034-4257\(03\)00100-7](https://doi.org/10.1016/S0034-4257(03)00100-7)
- Jain S.K. and Singh V.P., 2003. *Developments in water science*. Elsevier, Amst., The Netherlands, 5, 123-205, [https://doi.org/10.1016/S0167-5648\(03\)80057-6](https://doi.org/10.1016/S0167-5648(03)80057-6)
- Kamble B., Kilic A., and Hubbard K., 2013. Estimating crop coefficients using remote sensing-based vegetation index. *Remote Sens.*, 5(4), 1588-1602, <https://doi.org/10.3390/rs5041588>
- Lee K., Park C.W., Na S.I., Jung M.P., and Kim J., 2017. Monitoring on crop condition using remote sensing and model. *Korean J. Remote Sens.*, 33(5-2), 617-620, <https://doi.org/10.7780/kjrs.2017.33.5.2.1>
- Li F., Jupp D.L.B., Reddy S., Lymburner L., Mueller N., Tan P., and Islam A., 2010. An evaluation of the use of atmospheric and BRDF correction to standardize landsat data. *IEEE J. Sel. Top. Appl. Earth Obs. Remote Sens.*, 3(3), 257-270, <https://doi.org/10.1109/JSTARS.2010.2042281>
- Li W., Jiang J., Weiss M., Madec S., Tison F., Philippe B., Comar A., and Baret F., 2021. Impact of the reproductive organs on crop BRDF as observed from a UAV. *Remote Sens. Environ.*, 259(15), 112433, <https://doi.org/10.1016/j.rse.2021.112433>
- Liu H.Q. and Huete A.R., 1995. A feedback based modification of the NDVI to minimize canopy background and atmospheric noise. *IEEE Trans. Geosci. Remote Sens.*, 33, 457-465, <https://doi.org/10.1109/TGRS.1995.8746027>
- Ma D., Rehman T.U., Zhang L., Maki H., Tuinstra M.R., and Jin J., 2021. Modeling of diurnal changing patterns in airborne crop remote sensing images. *Remote Sens.*, 13(9), 1719, <https://doi.org/10.3390/rs13091719>
- Matsushita B., Yang W., Chen J., Onda Y., and Qiu G., 2007. Sensitivity of the enhanced vegetation index (EVI) and normalized difference vegetation index (NDVI) to topographic effects: a case study in high-density cypress forest. *Sensors*, 7(11), 2636-2651, <https://doi.org/10.3390/s7112636>
- Na S.I., Park C.W., Cheong Y.K., Kang C.S., Choi I.B., and Lee K.D., 2016. Selection of optimal vegetation indices for estimation of barley wheat growth based on remote sensing. *Korean J. Remote Sens.*, 32(5), 483-497, <https://doi.org/10.7780/kjrs.2016.32.5.7>
- Ortega-Terol D., Hernandez-Lopez D., Ballesteros R., and Gonzalez-Aguilera D., 2017. Automatic hotspot and sun glint detection in UAV multispectral images. *Sensors*, 17(10), 2352, <https://doi.org/10.3390/s17102352>
- Qiu B., Guo W., Xue Y., and Dai Q., 2016. Implementation and evaluation of a generalized radiative transfer scheme within canopy in the soil-vegetation-atmosphere transfer (SVAT) model. *J. Geophys. Res. Atmos.*, 121(20), 12145-12163, <https://doi.org/10.1002/2016JD025328>
- Queally N., Ye Z., Zheng T., Chlus A., Schneider F., Pavlick R.P., and Townsend P.A., 2022. FlexBRDF: A flexible BRDF correction for grouped processing of airborne imaging spectroscopy flightlines. *J. Geophys. Res.: Biogeosci.*, 127(1), e2021JG006622, <https://doi.org/10.1029/2021JG006622>
- Ryu J.H., Jeong H., and Cho J., 2020. Performances of vegetation indices on paddy rice at elevated air temperature, heat stress, and herbicide damage. *Remote Sens.*, 12(16), 2654, <https://doi.org/10.3390/rs12162654>
- Sandmeier S.R. and Itten K.I., 1999. A field goniometer system (FIGOS) for acquisition of hyperspectral BRDF data. *IEEE Trans. Geosci. Remote Sens.*, 37(2), 978-986, <https://doi.org/10.1109/36.752216>
- Schill S.R., Jensen J.R., Raber G.T., and Porter D.E., 2004. Temporal modeling of bidirectional reflection distribution function (BRDF) in coastal vegetation. *GISci. Remote Sens.*, 41(2), 116-135, <https://doi.org/10.2747/1548-1603.41.2.116>
- Shafian S., Rajan N., Schnell R., Bagavathiannan M., Valasek J., Shi Y., and Olsenholler J., 2018. Unmanned aerial systems-based remote sensing for monitoring sorghum growth and development. *PLoS one*, 13(5), e0196605, <https://doi.org/10.1371/journal.pone.0196605>
- Sharifi A., 2020. Using sentinel-2 data to predict nitrogen uptake in maize crop. *IEEE J. Sel. Top. Appl. Earth Obs. Remote Sens.*, 13, 2656-2662, <https://doi.org/10.1109/JSTARS.2020.2998638>
- Sinclair T.R. and Sheehy J.E., 1999. Erect leaves and photosynthesis in rice. *Science*, 283(5407), 1455-1455, <https://doi.org/10.1126/science.283.5407.1455>

- Sun T., Fand H., Liu W., and Ye Y., 2017. Impact of water background on canopy reflectance anisotropy of a paddy rice field from multi-angle measurements. *Agric. For. Meteorol.*, 233(15), 143-152, <https://doi.org/10.1016/j.agrformet.2016.11.010>
- Suomalainen J., Hakala T., Peltoniemi J., and Puttonen E., 2009. Polarised multiangular reflectance measurements using the finnish geodetic institute field goniospectrometer. *Sensors*, 9(5), 3891-3907, <https://doi.org/10.3390/s90503891>
- Towers P.C., and Poblete-Echeverría C., 2021. Effect of the illumination angle on NDVI data composed of mixed surface values obtained over vertical-shoot-positioned vineyards. *Remote Sens.*, 13(5), 855, <https://doi.org/10.3390/rs13050855>
- Yan J., Zhang G., Ling H., and Han F., 2022. Comparison of time-integrated NDVI and annual maximum NDVI for assessing grassland dynamics. *Ecol. Indic.*, 136, 108611, <https://doi.org/10.1016/j.ecolind.2022.108611>
- Zhang Q., Cheng Y.B., Lyapustin A.I., Wang Y., Xiao X., Suyker A., Verma S., Tan B., and Middleton E.M., 2014. Estimation of crop gross primary production (GPP): I. Impact of MODIS observation footprint and impact of vegetation BRDF characteristics. *Agric. For. Meteorol.*, 191(15), 51-63, <https://doi.org/10.1016/j.agrformet.2014.02.002>
- Zhang Y., Liu X., Su S., and Wang C., 2014. Retrieving canopy height and density of paddy rice from Radarsat-2 images with a canopy scattering model. *Int. J. Appl. Earth Obs. Geoinf.*, 28, 170-180, <https://doi.org/10.1016/j.jag.2013.12.005>